Online Simultaneous Identification of Multi-parameters for Interior PMSMs under Sensorless Control

Peng Wang, Z. Q. Zhu, *Fellow*, *IEEE*, N. M. A. Freire, Ziad Azar, Ximeng Wu, and Dawei Liang

***Abstract*—Under sensorless control, the position estimation error in interior permanent magnet (PM) synchronous machines will lead to parameter identification errors and a rank-deficiency issue. This paper proposes a parameter identification model that is independent of position error by combining the dq-axis voltage equations. Then, a novel dual signal alternate injection method is proposed to address the rank-deficiency issue, i.e., during one injection period, a zero, positive, and negative d-axis current injection together with a rotor position offset injection, to simultaneously identify the multi-parameters, including stator resistance, dq-axis inductances, and PM flux linkage. The proposed method is verified by experiments at different dq-axis current conditions.**

***Index Terms*—Current injection, Interior permanent magnet synchronous machines (IPMSMs), Online multi-parameter identification, Rotor position-offset injection, Sensorless control.**

I. Introduction

INTERIOR permanent magnet synchronous machines (IPMSMs) are widely used in electrical transportation and industrial servo drives, etc. [1]-[2]. The machine parameters, i.e., stator resistance, inductances, and permanent magnet (PM) flux linkage, are essential for PI parameter setting of current loops, maximum torque per ampere control, position sensorless control, and fault diagnosis, etc. [3]. Thus, it is necessary to perform an online multi-parameter identification.

For online multi-parameter identification based on rotor position sensor drive, various methods are developed, including adding additional measuring instruments [4] or additional harmonic model [5] and signal excitation [6]-[12]. However, the utilization of additional torque sensor in [4] and harmonic model [5] will limit the application scenarios. Moreover, extra signal excitation is often used to increase the number of equations, e.g., current injection [6]-[8], position-offset injection [9]-[11], and variable speed [12]. However, the above current or position-offset injection is still based on position-sensored control, which cannot be applied to sensorless control directly. Also, variable speed has changed the operation state of machines, which is only suitable for specific conditions.

Sensorless control eliminates mechanical position sensors and mainly includes saliency-based [13]-[14] and fundamental model-based [15]-[18] methods. The former relies on high-frequency signal injection and is effective at low speed for permanent magnet synchronous machines (PMSMs) with saliency, while the latter estimates rotor position from back-electromotive force (back-EMF) or flux linkage at medium and high speeds. However, model-based observers are highly sensitive to parameter variations. Under sensorless operation, the position error itself becomes an additional unknown, complicating accurate parameter identification [19]-[20] and also leading to rank-deficiency [6].

For the former, there are mainly two methods to overcome the influence of position observation error on parameter identification. Firstly, the identification model ignoring position error is utilized to identify parameters, and then, the identified parameters are fed back to the position observer to correct position error until both the identified parameters and position converge [21]. This will lead to “error transfer” issue [20], since the error of position estimation will cause the parameter identification error, and in turn, the parameter identification error also deteriorates the position estimation. At last, it is difficult to guarantee the convergence of the designed estimator under sensorless control.

Secondly, some methods focus on sensorless control, while parameter identification is only used as an auxiliary means to reduce position estimation errors [22]-[23]. Therefore, most of these methods utilize the special properties of various position observers [24]-[25], or only the parameters needed by position observer can be identified [26]-[27]. On the one hand, in [24]-[25], a sinusoidal current signal is injected into the d-axis to estimate stator resistance and inductance by utilizing the error between the observed and measured currents, which improves adaptive full-state feedback sensorless control. However,

Manuscript received August 11, 2025; revised September 08, 2025; accepted September 20, 2025. Date of publication December 25, 2025; Date of current version November 24, 2025.

Peng Wang is with the Department of Electronic and Electrical Engineering, The University of Manchester, Manchester M13 9PL, U.K. (e-mail: peng.wang-2@manchester.ac.uk).

Z. Q. Zhu is with the Department of Electrical and Electronic Engineering, The Hong Kong Polytechnic University, Hong Kong, China (e-mail: z.q.zhu@polyu.edu.hk).

N. M. A. Freire, Ziad Azar, and Ximeng Wu are with Siemens Gamesa Renewable Energy AS Ringgold standard institution, Aalborg, North Denmark Region 9220, Denmark (e-mail: Nuno.Freire@siemensgamesa.com; ziad.azar@siemensgamesa.com; ximeng.xw.wu@siemensgamesa.com).

Dawei Liang is with the Department of Electronic and Electrical Engineering, University of Sheffield, Sheffield, South Yorkshire S1 3JD, U.K. (e-mail: d.liang@ieee.org).

(Corresponding Author: Z. Q. Zhu)

Digital Object Identifier 10.30941/CESTEMS.2025.00029

under the reduced-order back-EMF observer, this method does not work. Even though some methods can be applied to all position observers, such as in [28]-[29], where the position error is identified as a parameter, and the rank-deficiency problem is solved by injecting dq-axis currents, it ignores the changes in position error caused by the signal injection. On the other hand, in [26], the online tracking of the minimum current vector is adopted to minimize the position error of sensorless control. Only stator resistance can be identified, but other parameters are set to a constant. Overall, although the parameter estimation under sensorless control has obtained great research interest in recent years, the detrimental effect of rotor position error on the parameter estimation needs to be further investigated.

For the latter, even by signal injection, the identification model will easily suffer from rank-deficiency because of the introduction of position error, which makes it impossible to identify multi-parameters simultaneously. To address the rank-deficiency issue, the injected signal should cause obvious variation of voltage terms containing the parameters to be identified, and the full-rank identification model denotes that the number of parameters should be equal to that of equations after signal injection [6], [30], [31]. Otherwise, the identified parameters will converge to the local optimal solution, instead of global optimal solution. Under sensorless control of PMSMs, there are five unknown parameters, i.e., resistance, d-, q-axis inductances, PM flux linkage, and position error, while the rank of identification model is two in synchronous reference frame (SRF). It is obvious that there is a rank-deficiency issue, which requires signal injection to add three additional independent equations.

For multi-parameter identification, the method of d-axis current injection is often utilized [24]-[25]. For d-axis current injection, the two parameters, i.e., resistance and d-axis inductance, can be identified accurately because of the obvious variation of voltage terms. Therefore, four independent equations can be constructed. However, there is still one parameter that cannot be identified, which shows that rank-deficiency issue is serious in online parameter identification under sensorless control by only d-axis current injection. For example, in [32], with the help of solving a multivariate nonlinear regression problem, the identification model of sensorless control of surface-mount permanent-magnet synchronous machines (SPMSMs) without position error is established, but the developed model only includes three independent equations with four unknown parameters by d-axis current injection. As a result, q-axis inductance and PM flux linkage are difficult to identify simultaneously.

Another injection method is position offset, which has been popular recently [9]-[11]. The d-axis voltage fluctuation is sampled to identify PM flux linkage independently by injecting a positive and a negative position offset [9]-[10]. However, position offset injection will only cause the obvious variation in voltage term of PM flux linkage, which will only construct three independent equations. Therefore, it cannot be used to simultaneously identify multiple parameters. Therefore, to the best knowledge of authors, up to date, it is difficult to simultaneously identify all parameters, including stator resistance, dq-axis inductances, and PM flux linkage, by only one kind of signal injection under sensorless control until now.

In order to achieve multi-parameter identification, the step-by-step identification method is often adopted [20], [33], [34]. For example, in [20], position offset is injected to estimated position to identify stator inductance under zero d-axis current control and stator resistance and PM flux linkage under non-zero d-axis current control. Stator resistance and dq-axis inductances are identified at standstill with current injection, and PM flux linkage is identified in operation state utilizing identified stator resistance and inductances [33]. But the stepwise method usually requires changing the operating condition of machine, and the parameters identified first may degrade the accuracy of subsequently identified parameters. Overall, under sensorless control, online simultaneous multi-parameter identification is a challenging research area and needs to be further investigated.

In this paper, under the fundamental model-based sensorless control, an online simultaneous multi-parameter identification method under sensorless control is proposed. There are two main features: 1) By combining dq-axis voltage equations, the proposed identification model has eliminated the position error term, resulting in suppressing the influence of position error on parameter identification. 2) It is revealed that the online multi-parameter identification under sensorless control easily suffers from a rank-deficiency issue since the unknown rotor position is introduced in the estimation, which results in multiple parameters being unable to be identified simultaneously. To address this issue, this paper proposes a novel dual signal alternate injection method, i.e., during one injection period, a zero, positive, and negative d-axis current injection together with a position offset injection to construct a full-rank identification model. By sampling voltages and currents, the parameters, including stator resistance, dq-axis inductances, and PM flux linkage, can be identified simultaneously utilizing a gradient descent-based least square algorithm.

The rest of paper is organized as follows. Section II introduces the least-order observer of sensorless control. In Section III, the influences of position error and rank-deficiency issue on online simultaneous identification of multi-parameters are analysed. In Section IV, utilizing developed identification model, the proposed dual signal alternate injection method is presented. The experimental results are given in Section V. Finally, conclusions are drawn in Section VI.

II. EXTENDED-EMF BASED SENSORLESS CONTROL

A. Mathematical Model

The mathematical model of IPMSM in SRF is given as (1):

$$\begin{bmatrix} u_\mathrm{d} \\ u_\mathrm{q} \end{bmatrix} = \begin{bmatrix} R + pL_\mathrm{d} & -\omega_\mathrm{r} L_\mathrm{q} \\ \omega_\mathrm{r} L_\mathrm{q} & R + pL_\mathrm{d} \end{bmatrix} \begin{bmatrix} i_\mathrm{d} \\ i_\mathrm{q} \end{bmatrix} + \begin{bmatrix} 0 \\ E_\mathrm{ex} \end{bmatrix} \tag{1}$$

where $E_\mathrm{ex} = \omega_\mathrm{r}\psi_\mathrm{m} + (L_\mathrm{d} - L_\mathrm{q})(\omega_\mathrm{r} i_\mathrm{d} - pi_\mathrm{q})$, known as extended-EMF. L_d, L_q, R, and ψ_m are the actual dq-axis inductances, the stator resistance, and the PM flux linkage, respectively. p

is the differential operator. ω_{r} is the electrical angular speed. i_{d}, i_{q}, u_{d}, and u_{q} are the d-, q-axis currents and voltages, respectively.

For a sensorless control system, the above model should be transformed to the estimated SRF, as expressed in (2) and (3) [35]:

$$\begin{bmatrix} u_{\mathrm{d}}^{\mathrm{e}} \\ u_{\mathrm{q}}^{\mathrm{e}} \end{bmatrix} = \begin{bmatrix} R + pL_{\mathrm{d}} & -\omega_{\mathrm{r}}^{\mathrm{e}} L_{\mathrm{q}} \\ \omega_{\mathrm{r}}^{\mathrm{e}} L_{\mathrm{q}} & R + pL_{\mathrm{d}} \end{bmatrix} \begin{bmatrix} i_{\mathrm{d}}^{\mathrm{e}} \\ i_{\mathrm{q}}^{\mathrm{e}} \end{bmatrix} + \begin{bmatrix} E_{\mathrm{d}}^{\mathrm{e}} \\ E_{\mathrm{q}}^{\mathrm{e}} \end{bmatrix} \tag{2}$$

$$\begin{bmatrix} E_{\mathrm{d}}^{\mathrm{e}} \\ E_{\mathrm{q}}^{\mathrm{e}} \end{bmatrix} = E_{\mathrm{ex}} \begin{bmatrix} -\sin \Delta\theta_{\mathrm{r}} \\ \cos \Delta\theta_{\mathrm{r}} \end{bmatrix} + \Delta\omega_{\mathrm{r}} L_{\mathrm{q}} \begin{bmatrix} i_{\mathrm{q}}^{\mathrm{e}} \\ -i_{\mathrm{d}}^{\mathrm{e}} \end{bmatrix} \tag{3}$$

where the superscript sign "e" indicates that the variables are in the estimated SRF, $\Delta\theta_{\mathrm{r}}$ is the position estimation error, and $\Delta\omega_{\mathrm{r}} = \omega_{\mathrm{r}}^{\mathrm{e}} - \omega_{\mathrm{r}}$. $E_{\mathrm{d}}^{\mathrm{e}}$ and $E_{\mathrm{q}}^{\mathrm{e}}$ are the d-, q-axis extended-EMF in the estimated SRF. The estimated rotor speed ($\omega_{\mathrm{r}}^{\mathrm{e}}$) is controlled in the observer to follow the actual speed (ω_{r}) in sensorless controlled IPMSM. Therefore, the error $\Delta\omega_{\mathrm{r}}$ is zero in (3).

B. Rotor Position Observer of IPMSM

The least-order observer can be constructed by selecting the state variable $\boldsymbol{i}_{\mathrm{dq}} = [i_{\mathrm{d}}^{\mathrm{e}}, i_{\mathrm{q}}^{\mathrm{e}}]^{\mathrm{T}}$, as stated in (4):

$$p\boldsymbol{i}_{\mathrm{dq}} = \tilde{\boldsymbol{A}}_{11}\boldsymbol{i}_{\mathrm{dq}} + \tilde{\boldsymbol{A}}_{12}\hat{\boldsymbol{E}}_{\mathrm{dq}} + \tilde{\boldsymbol{B}}\tilde{\boldsymbol{u}}_{\mathrm{dq1}} \tag{4}$$

where

$$\begin{gathered} \tilde{\boldsymbol{u}}_{\mathrm{dq1}} = \begin{bmatrix} u_{\mathrm{d}}^{\mathrm{e}} + \omega_{\mathrm{r}}^{\mathrm{e}} \tilde{L}_{\mathrm{q}} i_{\mathrm{q}}^{\mathrm{e}} & u_{\mathrm{q}}^{\mathrm{e}} - \omega_{\mathrm{r}}^{\mathrm{e}} \tilde{L}_{\mathrm{q}} i_{\mathrm{d}}^{\mathrm{e}} \end{bmatrix}^{\mathrm{T}} \\ \tilde{\boldsymbol{A}}_{11} = -\frac{\tilde{R}}{\tilde{L}_{\mathrm{d}}}\boldsymbol{I}, \tilde{\boldsymbol{A}}_{12} = -\frac{1}{\tilde{L}_{\mathrm{d}}}\boldsymbol{I}, \tilde{\boldsymbol{B}} = \frac{1}{\tilde{L}_{\mathrm{d}}}\boldsymbol{I}, \boldsymbol{I} = \begin{bmatrix} 1 & 0 \\ 0 & 1 \end{bmatrix} \end{gathered} \tag{5}$$

where $\hat{\boldsymbol{E}}_{\mathrm{dq}} = [\hat{E}_{\mathrm{d}}^{\mathrm{e}}, \hat{E}_{\mathrm{q}}^{\mathrm{e}}]^{\mathrm{T}}$ is the estimated extended-EMF, and the superscript "~" denotes the reference value. $\boldsymbol{u}_{\mathrm{dq1}}$ denotes the compensated stator voltage vector in the estimated SRF, obtained by removing the cross-coupling terms from $u_{\mathrm{d}}^{\mathrm{e}}$ and $u_{\mathrm{q}}^{\mathrm{e}}$. $\boldsymbol{A}_{11}$, $\boldsymbol{A}_{12}$, and $\boldsymbol{B}$ are the system matrices of the least-order extended-EMF observer. Fig. 1 shows the equivalent block diagram of the least-order extended-EMF observer for estimating $\boldsymbol{E}_{\mathrm{dq}}$ and phase locked loop (PLL) for estimating position and speed. The rotor position error is expressed as (6):

$$\Delta\hat{\theta}_{\mathrm{r}} = \tan^{-1}\left(-\hat{E}_{\mathrm{d}}^{\mathrm{e}}/\hat{E}_{\mathrm{q}}^{\mathrm{e}}\right) \tag{6}$$

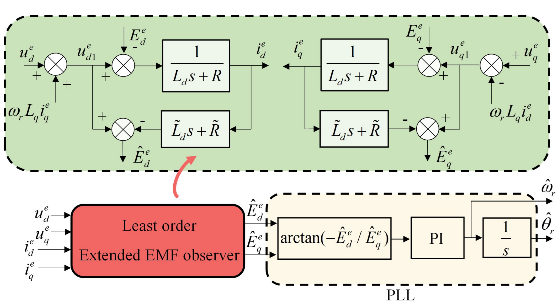

Fig. 1. Equivalent block diagram of least-order extended-EMF observer and PLL.

The position estimation error is mainly caused by parameter errors of stator resistance and inductance [27]-[36], as expressed in (7):

$$\sin\Delta\theta_{\mathrm{r\_R}} = \frac{\Delta R}{E_{\mathrm{ex}}} i_{\mathrm{d}}^{\mathrm{e}}, \ \sin\Delta\theta_{\mathrm{r}\_L_{\mathrm{q}}} = \frac{-\Delta L_{\mathrm{q}}\omega_{\mathrm{r}}}{E_{\mathrm{ex}}} i_{\mathrm{q}}^{\mathrm{e}}, \ \sin\Delta\theta_{\mathrm{r}\_L_{\mathrm{d}}} = 0 \tag{7}$$

where $\Delta\theta_{\mathrm{r\_R}}$, $\Delta\theta_{\mathrm{r}\_L_{\mathrm{d}}}$, and $\Delta\theta_{\mathrm{r}\_L_{\mathrm{q}}}$ represent the position estimation errors caused by errors of stator resistance, d-, and q-axis inductances, respectively.

III. Issues of Online Multi-parameter Identification under Sensorless Control

In this section, the influence of position error on parameter identification is discussed. Then, it is revealed that simultaneous identification of multi-parameters easily suffers from rank deficiency because of the introduction of unknown rotor position.

A. Influence of Position Error on Multi-parameter Identification

According to (7), the unknown R and L_{q} will lead to position estimation error, which will, in turn, deteriorate the accuracy of parameter identification. The parameter identification model without considering the influence of position error [21] can be used as an example to demonstrate the influence of position estimation error. The multi-parameter identification model before and after d-axis current injection can be expressed by (8a) and (8b):

$$\begin{aligned} u_{\mathrm{d1}}^{\mathrm{e}} &= -\omega_{\mathrm{r}} L_{\mathrm{q}} i_{\mathrm{q1}}^{\mathrm{e}} - E_{\mathrm{ex1}} \sin\left(\Delta\theta_{\mathrm{r1}}\right) \\ u_{\mathrm{q1}}^{\mathrm{e}} &= R i_{\mathrm{q1}}^{\mathrm{e}} + E_{\mathrm{ex1}} \cos\left(\Delta\theta_{\mathrm{r1}}\right) \end{aligned} \tag{8a}$$

$$\begin{aligned} u_{\mathrm{d2}}^{\mathrm{e}} &= R i_{\mathrm{d2}}^{\mathrm{e}} - \omega_{\mathrm{r}} L_{\mathrm{q}} i_{\mathrm{q2}}^{\mathrm{e}} - E_{\mathrm{ex2}} \sin\left(\Delta\theta_{\mathrm{r2}}\right) \\ u_{\mathrm{q2}}^{\mathrm{e}} &= R i_{\mathrm{q2}}^{\mathrm{e}} + \omega_{\mathrm{r}} L_{\mathrm{q}} i_{\mathrm{d2}}^{\mathrm{e}} + E_{\mathrm{ex2}} \cos\left(\Delta\theta_{\mathrm{r2}}\right) \end{aligned} \tag{8b}$$

where the subscripts 1 and 2 represent without and with d-axis current injection, respectively. Thus, R, ψ_{m}, L_{d}, and L_{q} identification will be implemented according to (8a) and (8b), as shown in (9):

$$\begin{aligned} L_{\mathrm{d}} &= \frac{u_{\mathrm{d1}}^{\mathrm{e}} + \cos^2\left(\Delta\theta_{\mathrm{r1}}\right)\omega_{\mathrm{r}} L_{\mathrm{q}} i_{\mathrm{q1}}^{\mathrm{e}} + \omega_{\mathrm{r}}\psi_{\mathrm{m}}\sin\left(\Delta\theta_{\mathrm{r1}}\right)}{\omega_{\mathrm{r}} i_{\mathrm{q1}}^{\mathrm{e}} \sin^2\left(\Delta\theta_{\mathrm{r1}}\right)} \\ L_{\mathrm{q}} &= -\frac{u_{\mathrm{d1}}^{\mathrm{e}}}{\omega_{\mathrm{r}} i_{\mathrm{q1}}^{\mathrm{e}}} - \frac{E_{\mathrm{ex1}}\sin\left(\Delta\theta_{\mathrm{r1}}\right)}{\omega_{\mathrm{r}} i_{\mathrm{q1}}^{\mathrm{e}}} \\ R &= \frac{u_{\mathrm{d2}}^{\mathrm{e}} + \omega_{\mathrm{r}} L_{\mathrm{q}} i_{\mathrm{q2}}^{\mathrm{e}}}{i_{\mathrm{d2}}^{\mathrm{e}}} + \frac{E_{\mathrm{ex1}}\sin\left(\Delta\theta_{\mathrm{r2}}\right)}{i_{\mathrm{d2}}^{\mathrm{e}}} \\ \psi_{\mathrm{m}} &= \frac{u_{\mathrm{q1}}^{\mathrm{e}} - R i_{\mathrm{q1}}^{\mathrm{e}}}{\omega_{\mathrm{r}}\cos\left(\Delta\theta_{\mathrm{r1}}\right)} - \left(L_{\mathrm{d}} - L_{\mathrm{q}}\right) i_{\mathrm{q1}}^{\mathrm{e}} \sin\left(\Delta\theta_{\mathrm{r1}}\right) \end{aligned} \tag{9}$$

In (9), the four parameters, i.e., L_{d}, L_{q}, R, and ψ_{m} are all influenced by the position error $\Delta\theta_{\mathrm{r}}$. Therefore, under position sensorless control, the conventional identification model cannot be utilized for multi-parameter identification.

B. Rank-deficiency Issue under Sensorless Control

Table I compares the multi-parameter identification between position sensor and sensorless control by single current injection and single position offset injection. For the control system with a position sensor, there are four parameters, but only two identification equations in SRF [6]. In terms of d-axis current injection, L_d, L_q, R, and ψ_m are identified according to voltage terms $\omega_r L_d i_d$, $\omega_r L_q i_q$, Ri_d (Ri_q), $\omega_r \psi_m$, respectively. When injecting current in d-axis, there are obvious variations of voltage terms, including $\omega_r L_d i_d$ and Ri_d. L_d and R can be identified with d-axis current injection, which constructs four independent equations. According to the discussion on rank-deficiency in Section I, all parameters including L_d, L_q, R, and ψ_m can be identified. As for position offset injection $(\pm\Delta\theta_\delta)$, L_d, L_q, R, and ψ_m are identified according to voltage terms $\omega_r L_d i_d$, $\omega_r L_q i_q$, Ri_d, (Ri_q), $\pm\omega_r \psi_m \sin\Delta\theta_\delta$, respectively. Therefore, ψ_m can be identified by positive and negative position offset injections [9]. Combining with the two equations before position offset injection, three parameters can be identified accurately. Therefore, it is straightforward to address the rank-deficiency issue of online multi-parameter identification to the control system with a rotor position sensor only by a single current injection or single position offset injection.

TABLE I
COMPARISON OF MULTI-PARAMETER IDENTIFICATION BETWEEN POSITION SENSOR AND SENSORLESS CONTROL BY SINGLE SIGNAL INJECTION

		Position sensor control	Position sensorless control
Number of parameters		4	5
Current injection	Rank	2	
	Identified parameter	2 (L_d, R)	
	Independent equations	4	
	Unidentifiable	0	1
Pos. offset injection	Identified parameter	1 (ψ_m)	
	Independent equations	3	
	Unidentifiable	1	2

However, under position sensorless control, due to the introduction of unknown position, there are five unknown parameters including L_d, L_q, R, ψ_m, and $\Delta\theta_r$, as shown in Table I. d-axis current injection can be only utilized to identify two parameters including L_d and R to construct four independent equations, and position offset injection can be only utilized to identify ψ_m to construct three independent equations, which all leads to the issue of rank-deficiency. L_d, L_q, R, and ψ_m cannot be simultaneously identified by single current or position offset injection under position sensorless control, as shown in Table I. Therefore, in this paper, a dual signal alternate injection method is proposed to solve rank-deficiency issue, which will be discussed in part B of Section IV.

IV. PROPOSED ONLINE MULTI-PARAMETER IDENTIFICATION

In this section, the multi-parameter identification model without position estimation error is proposed by combining dq-axis voltage equations. Moreover, rank-deficiency issue is addressed by dual signal alternate injection to identify multi parameters simultaneously. Finally, the amplitude selection of signal injection is presented.

A. Proposed Identification Model without Influence of Position Error

Parameter identification model of PMSM is written as (10a) and (10b):

$$\begin{bmatrix} u_d^e \\ u_q^e \end{bmatrix} = \begin{bmatrix} R & -\omega_r L_q \\ \omega_r L_q & R \end{bmatrix} \begin{bmatrix} i_d^e \\ i_q^e \end{bmatrix} + E_{ex} \begin{bmatrix} \sin(-\Delta\theta_r) \\ \cos(\Delta\theta_r) \end{bmatrix} \tag{10a}$$

$$E_{ex} = \omega_r \psi_m + (L_d - L_q)\omega_r i_d \tag{10b}$$

where $i_d = i_d^e \cos(\Delta\theta_r) + i_q^e \sin(\Delta\theta_r)$. Because $\Delta\theta_r$ is a small value, it is reasonable to assume that $\cos\Delta\theta_r \approx 1$. Therefore, (10) can be expressed as (11a) and (11b):

$$\begin{aligned} u_d^e = Ri_d^e - \omega_r L_q i_q^e - \omega_r \psi_m \sin(\Delta\theta_r) - \\ \omega_r (L_d - L_q)\left(i_d^e + i_q^e \sin(\Delta\theta_r)\right)\sin(\Delta\theta_r) \end{aligned} \tag{11a}$$

$$u_q^e = Ri_q^e + \omega_r L_q i_d^e + \omega_r \psi_m + \omega_r (L_d - L_q)\left(i_d^e + i_q^e \sin(\Delta\theta_r)\right) \tag{11b}$$

(11b) × sin($\Delta\theta_r$) − (11a) is given by (12):

$$\sin(\Delta\theta_r) = \frac{u_d^e - Ri_d^e + \omega_r L_q i_q^e}{-u_q^e + Ri_q^e + \omega_r L_q i_d^e} \tag{12}$$

Substituting (12) into (11b) yields the parameter identification model, as shown in (13):

$$\begin{aligned} f(L_d, L_q, R, \psi_m) = -u_q^e + Ri_q^e + \omega_r L_d i_d^e + \omega_r \psi_m + \\ (L_d - L_q)\omega_r i_q^e \frac{u_d^e - Ri_d^e + \omega_r L_q i_q^e}{-u_q^e + Ri_q^e + \omega_r L_q i_d^e} \\ = 0 \end{aligned} \tag{13}$$

Due to no position error term in (13), the influence of position error on multi-parameter identification is suppressed. It should be noted that (13) is an accurate identification model if there is no position estimation error after identified parameters are fed back to position observer.

It is worth noting that the parameter identification model in (13) is derived from the mathematical model in the estimated SRF in (10). Both the extended-EMF observer and the flux observer are based on the fundamental model (10). Therefore, the proposed method is suitable for both extended-EMF and flux observers.

B. Proposed Dual Signal Alternate Injection Method for Online Multi-parameter Identification

As discussed in part B of Section III, L_d, L_q, R, and ψ_m cannot be simultaneously identified by single current or position offset injection under position sensorless control due to rank-deficiency issue. Thus, a dual signal alternate injection method is proposed to solve rank-deficiency issue in this paper, i.e., d-axis current injection together with position offset injection, and the feature is outlined in Table II.

As can be seen from parameter identification model in (13), there are four parameters but only with one equation.

TABLE II
COMPARISON OF RANK-DEFICIENCY ISSUE BETWEEN PROPOSED AND SINGLE SIGNAL INJECTION METHODS

Identified parameters	**d-axis current injection**		**Position offset injection**		**Proposed dual signal alternate injection**	
	Voltage terms	Identification	Voltage terms	Identification	Voltage terms	Identification
$\boldsymbol{L_d}$	$\omega_r L_d i_d^e$	√	$\omega_r L_d i_d^e$	×	$\omega_r L_d i_d^e$	√
$\boldsymbol{L_q}$	$\omega_r L_q i_q^e$	×	$\omega_r L_q i_q^e$	×	$\omega_r L_q i_q^e$	√
$\boldsymbol{R}$	$Ri_d^e(Ri_q^e)$	√	$Ri_d^e(Ri_q^e)$	×	$Ri_d^e(Ri_q^e)$	√
$\boldsymbol{\psi_m}$	$\omega_r \psi_m$	×	$\pm\omega_r \psi_m \sin(\Delta\theta_\delta)$	√	$\pm\omega_r \psi_m \sin(\Delta\theta_\delta)$	√

"√": Capable of identification. "×": Incapable of identification.

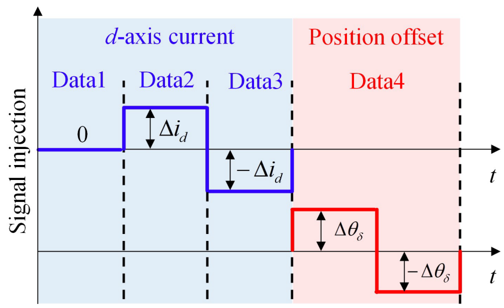

Fig. 2. Injection sequence of proposed dual signal alternate injection method for parameter identification.

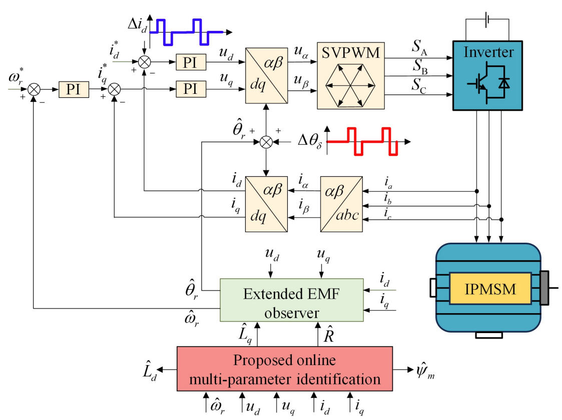

Fig. 3. Block diagram of proposed multi-parameter identification method.

Therefore, extra three equations need to be constructed by signal injection. The injection sequence of the proposed dual signal alternate injection method is shown in Fig. 2, and Fig. 3 shows the whole block diagram of proposed multi-parameter identification.

As shown in Fig. 2, zero, Δi_d, and $-\Delta i_\mathrm{d}$ are injected into d-axis current to construct three equations, and the corresponding data, i.e., voltages and currents, are sampled as data 1, data 2, and data 3, respectively. Then, $\pm\Delta\theta_\delta$ are injected into estimated rotor position to construct the fourth equation, and the corresponding data are sampled as data 4. The full-rank multi-parameter identification model can be established by the sampled data 1, data 2, data 3, and data 4, as expressed in (14):

$$\begin{cases} f_1\left(L_\mathrm{d}, L_\mathrm{q}, R, \psi_\mathrm{m}\right)=0 \\ f_2\left(L_\mathrm{d}, L_\mathrm{q}, R, \psi_\mathrm{m}\right)=0 \\ f_3\left(L_\mathrm{d}, L_\mathrm{q}, R, \psi_\mathrm{m}\right)=0 \\ f_4\left(L_\mathrm{d}, L_\mathrm{q}, R, \psi_\mathrm{m}\right)=0 \end{cases} \tag{14}$$

After identification model in (14) is developed, nonlinear recursive least square (RLS) algorithm based on gradient descent method is utilized for simultaneously identifying four parameters, i.e., L_d, L_q, R, and ψ_m. This RLS algorithm is simple and computationally efficient, which is essentially a regression estimation method that obtains a mathematical model fitting the sampled data to the minimum variance level.

After n sets of sample data (data 1–data 4) are obtained, i.e., currents, voltages, and rotor speed. The i-th equation of identification model can be described as (15):

$$\begin{aligned} f_i(\boldsymbol{x}) = &-\bar{u}_{\mathrm{q}i}^\mathrm{e} + x_3\bar{i}_{\mathrm{q}i}^\mathrm{e} + x_1\bar{i}_{\mathrm{d}i}^\mathrm{e}\bar{\omega}_{ri} + x_4\bar{\omega}_{ri} + \\ &\left(x_1 - x_2\right)\bar{i}_{\mathrm{q}i}^\mathrm{e}\bar{\omega}_{ri}\frac{\bar{u}_{\mathrm{d}i}^\mathrm{e} - x_3\bar{i}_{\mathrm{d}i}^\mathrm{e} + x_2\bar{i}_{\mathrm{q}i}^\mathrm{e}\bar{\omega}_{ri}}{-\bar{u}_{\mathrm{q}i}^\mathrm{e} + x_3\bar{i}_{\mathrm{q}i}^\mathrm{e} + x_2\bar{i}_{\mathrm{d}i}^\mathrm{e}\bar{\omega}_{ri}} \end{aligned} \tag{15a}$$

$$\boldsymbol{x} = \left[L_\mathrm{d}\ L_\mathrm{q}\ R\ \psi_\mathrm{m}\right]^\mathrm{T} \tag{15b}$$

where i = 1, 2, ... , n, $\boldsymbol{x}$ is the parameter identification vector, and the superscript "$-$" denotes the values after filtering.

The implementation of identification procedure is as follows:

1) Initialize N_iter = 30, c = 0.9, m = 0, where N_iter is the number of iteration times, c is the gradient factor which is within (0, 1), m is the cumulative number.

2) The error vector can be written as (16):

$$\Delta\boldsymbol{\varepsilon} = \left[f_1(\hat{\boldsymbol{x}})\ f_2(\hat{\boldsymbol{x}}), \ldots, f_n(\hat{\boldsymbol{x}})\right]^\mathrm{T} \tag{16}$$

where the superscript "^" denotes the identified value. The more accurate parameter identification indicates the smaller square sum of $\Delta\boldsymbol{\varepsilon}$, and thus, the cost function is expressed as (17):

$$S(\hat{\boldsymbol{x}}) = \Delta\boldsymbol{\varepsilon}^\mathrm{T}\Delta\boldsymbol{\varepsilon} \tag{17}$$

The goal of the parameter identification method is to find the best parameter vector $\hat{\boldsymbol{x}}$ to minimize the cost function.

3) The next is to calculate gradient vector. $\boldsymbol{\beta}(k)$ is the 4×1 gradient vector at the kth iteration, as shown in (18):

$$\hat{\boldsymbol{\beta}}(k) = \left(\boldsymbol{Z}(k)^\mathrm{T}\boldsymbol{Z}(k)\right)^{-1}\boldsymbol{Z}(k)^\mathrm{T}\Delta\boldsymbol{\varepsilon}(k) \tag{18}$$

In (18), the Jacobian matrix $\boldsymbol{Z}(k)$ is equal to (19):

$$\boldsymbol{Z}(k)_{ij} = \left.\frac{\partial f_i(\boldsymbol{x})}{\partial x_j}\right|_{\boldsymbol{x}=\hat{\boldsymbol{x}}(k)} \quad (i = 1, 2, \ldots, n,\ j = 1, 2, 3, 4) \tag{19}$$

where k = 1, 2, …, N_iter. j represents the four parameters. The specific calculation $\boldsymbol{Z}(k)_i$ can be expressed by (20a) as:

$$\frac{\partial f_i(\boldsymbol{x})}{\partial L_{\mathrm{d}}}=\varpi_{\mathrm{r}i}\bar{i}_{\mathrm{d}i}^{\mathrm{e}}+\varpi_{\mathrm{r}i}\bar{i}_{\mathrm{q}i}^{\mathrm{e}}\frac{\bar{u}_{\mathrm{d}i}^{\mathrm{e}}-\hat{R}(k)\bar{i}_{\mathrm{d}i}^{\mathrm{e}}+\varpi_{\mathrm{r}i}\hat{L}_{\mathrm{q}}(k)\bar{i}_{\mathrm{q}i}^{\mathrm{e}}}{-\bar{u}_{\mathrm{q}i}^{\mathrm{e}}+\hat{R}(k)\bar{i}_{\mathrm{q}i}^{\mathrm{e}}+\varpi_{\mathrm{r}i}\hat{L}_{\mathrm{q}}(k)\bar{i}_{\mathrm{d}i}^{\mathrm{e}}} \tag{20a}$$

$$\begin{aligned}\frac{\partial f_i(\boldsymbol{x})}{\partial L_{\mathrm{q}}}=&-\varpi_{\mathrm{r}i}\bar{i}_{\mathrm{q}i}^{\mathrm{e}}\frac{\bar{u}_{\mathrm{d}i}^{\mathrm{e}}-\hat{R}(k)\bar{i}_{\mathrm{d}i}^{\mathrm{e}}+\varpi_{\mathrm{r}i}\hat{L}_{\mathrm{q}}(k)\bar{i}_{\mathrm{q}i}^{\mathrm{e}}}{-\bar{u}_{\mathrm{q}i}^{\mathrm{e}}+\hat{R}(k)\bar{i}_{\mathrm{q}i}^{\mathrm{e}}+\varpi_{\mathrm{r}i}\hat{L}_{\mathrm{q}}(k)\bar{i}_{\mathrm{d}i}^{\mathrm{e}}}+\\&\left[\hat{L}_{\mathrm{d}}(k)-\hat{L}_{\mathrm{q}}(k)\right]\varpi_{\mathrm{r}i}^{2}\bar{i}_{\mathrm{q}i}^{\mathrm{e}}\times\\&\frac{-(\bar{u}_{\mathrm{d}i}^{\mathrm{e}}\bar{i}_{\mathrm{d}i}^{\mathrm{e}}+\bar{u}_{\mathrm{q}i}^{\mathrm{e}}\bar{i}_{\mathrm{q}i}^{\mathrm{e}})+\hat{R}(k)(\bar{i}_{\mathrm{d}i}^{\mathrm{e}2}+\bar{i}_{\mathrm{q}i}^{\mathrm{e}2})}{(-\bar{u}_{\mathrm{q}i}^{\mathrm{e}}+\hat{R}(k)\bar{i}_{\mathrm{q}i}^{\mathrm{e}}+\varpi_{\mathrm{r}i}\hat{L}_{\mathrm{q}}(k)\bar{i}_{\mathrm{d}i}^{\mathrm{e}})^2}\end{aligned} \tag{20b}$$

$$\begin{aligned}\frac{\partial f_i(\boldsymbol{x})}{\partial R}=&\,\bar{i}_{\mathrm{q}i}^{\mathrm{e}}-\frac{\varpi_{\mathrm{r}i}\bar{i}_{\mathrm{q}i}^{\mathrm{e}}(\hat{L}_{\mathrm{d}}(k)-\hat{L}_{\mathrm{q}}(k))(\bar{u}_{\mathrm{d}i}^{\mathrm{e}}\bar{i}_{\mathrm{q}i}^{\mathrm{e}}-\bar{u}_{\mathrm{q}i}^{\mathrm{e}}\bar{i}_{\mathrm{d}i}^{\mathrm{e}})}{(-\bar{u}_{\mathrm{q}i}^{\mathrm{e}}+\hat{R}(k)\bar{i}_{\mathrm{q}i}^{\mathrm{e}}+\varpi_{\mathrm{r}i}\hat{L}_{\mathrm{q}}(k)\bar{i}_{\mathrm{d}i}^{\mathrm{e}})^2}-\\&\frac{\varpi_{\mathrm{r}i}^{2}\bar{i}_{\mathrm{q}i}^{\mathrm{e}}(\hat{L}_{\mathrm{d}}(k)-\hat{L}_{\mathrm{q}}(k))\hat{L}_{\mathrm{q}}(k)(\bar{i}_{\mathrm{d}i}^{\mathrm{e}2}+\bar{i}_{\mathrm{q}i}^{\mathrm{e}2})}{(-\bar{u}_{\mathrm{q}i}^{\mathrm{e}}+\hat{R}(k)\bar{i}_{\mathrm{q}i}^{\mathrm{e}}+\varpi_{\mathrm{r}i}\hat{L}_{\mathrm{q}}(k)\bar{i}_{\mathrm{d}i}^{\mathrm{e}})^2}\end{aligned} \tag{20c}$$

$$\frac{\partial f_i(\boldsymbol{x})}{\partial \psi_{\mathrm{m}}}=\varpi_{\mathrm{r}i} \tag{20d}$$

4) Moreover, it is the rule for changing m. By calculating $f(\boldsymbol{a}_i, \hat{\boldsymbol{x}}(k+1))$ and $S(\hat{\boldsymbol{x}}(k+1))$, the natural variable will change as $m = m + 1$ if $S(\hat{\boldsymbol{x}}(k+1)) > S(\hat{\boldsymbol{x}}(k))$.

5) Finally, the iteration equation is written as (21):

$$\hat{\boldsymbol{x}}(k+1)=\hat{\boldsymbol{x}}(k)+c^{m}\hat{\boldsymbol{\beta}}(k) \tag{21}$$

The vector $\hat{\boldsymbol{x}}$ contains parameters to be identified including $L_{\mathrm{d}}, L_{\mathrm{q}}, R$, and ψ_{m}. Identified L_{q} and R can be fed back to position observer to correct position error. After several iterations, until the identified parameters maintain constant, it can be considered that the identified parameters are global optimal solution. The flowchart of proposed multi-parameter identification method is shown in Fig. 4.

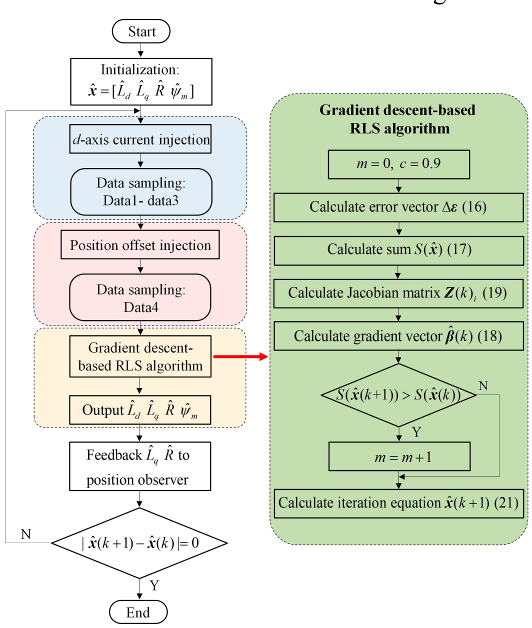

Fig. 4. Flowchart of proposed multi-parameter identification method.

C. Amplitude Selection of Signal Injection

The injected amplitude of d-axis current and position offset should not only be as small as possible to keep drive system stable, but also be large enough to make a large value of voltage terms related to estimated parameters to obtain a higher signal-to-noise ratio (SNR).

On the one hand, the influence of the stator resistance error on position observation can be derived as (7) to determine the upper limit of injected d-axis current. If the initial stator resistance in the position observer is 0, the position error has an upper limit ($\Delta\theta_{\mathrm{r\_max}}$) to prevent the operation efficiency reduction and system instability caused by the large error of position observation. Thus,

$$\Delta i_{\mathrm{d}} \le \Delta\theta_{\max}\frac{E_{\mathrm{ex}}}{R} \tag{22}$$

Fig. 5(a) shows a schematic diagram of selecting current injection amplitude. With the increase in rotor speed, the upper limit of current injection becomes higher. As can be seen from Fig. 5(b), the upper limit of current injection amplitude will also increase with increasing uppers of position error.

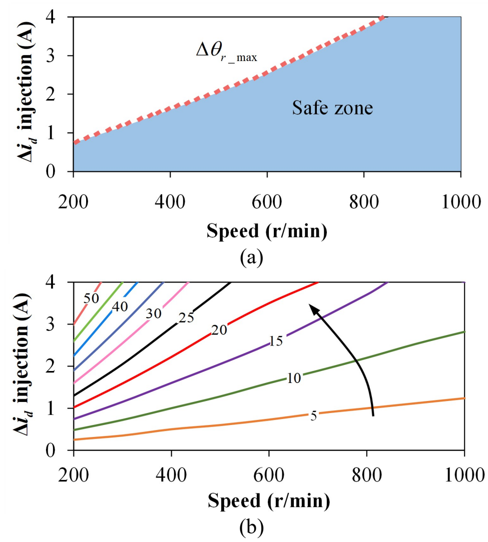

Fig. 5. Safe zone at different amplitudes of current injection. (a) Specific upper limit of position observation error. (b) Different upper limits of position error.

By the PI parameter selection of current loop, the upper limit of injected position offset can be confirmed. The typical current loop block diagram is shown in Fig. 6(a). In the diagram, T_{l} is the electric magnetic time constant, T_{ic} is the filtering time constant, and the inverter is simplified as a first-order inertial with time constant as T_{PWM}. After position offset is injected, the reference position of q-axis voltage and current vector changes, and the new block diagram is shown as Fig. 6(b). α is the angle between voltage vector and d-axis. After the equivalent transformation, the schematic block diagram is shown in Fig. 6(c), and two small inertial groups are composed into one inertial link $T_{\Sigma i} = T_{\mathrm{PWM}} + T_{\mathrm{ic}}$. Fig. 6(c) shows that the control object of the current loop is a dual inertia link, and the PI regulator can be utilized to simplify current loop as I-type. Its transfer function is written as (23):

$$W_{\mathrm{ACR}}(s)=\frac{K_{\mathrm{p}}(\tau_{\mathrm{i}}s+1)}{\tau_{\mathrm{i}}s} \tag{23}$$

where K_p and τ_i are the proportional gain and the integral time constant, respectively; s is the Laplace complex frequency variable. As shown in Fig. 6(d), the current loop is constructed as the typical I-type with selecting $\tau_i = T_1$. The open loop transfer function in Fig. 6(d) is shown as (24)):

$$G(s)H(s) = \frac{K_I \sec\Delta\theta_\delta}{s(1+T_{\Sigma i}s)} \tag{24}$$

where sec(·) denotes the secant function, and:

$$K_I = \frac{K_p K_{PWM} \csc\alpha \sin(\alpha - \Delta\theta_\delta)}{R\tau_i} \tag{25}$$

where csc(·) denotes the cosecant function, K_{PWM} represents the steady-state gain of the inverter, K_I denotes the equivalent gain.

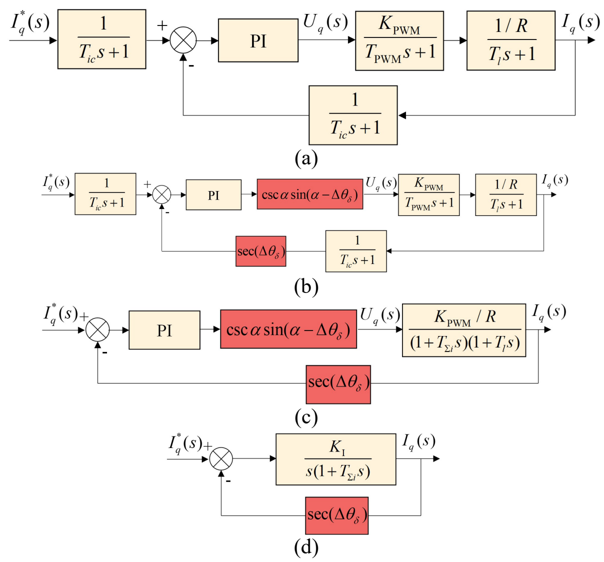

Fig. 6. Schematic block diagram of current loop. (a) Before injection. (b) After injection. (c) Equivalent transformation. (d) Equivalent transformation into I-type.

According to log magnitude-frequency characteristics of (24), the curve should cross the 0 dB line with a ratio of −20 dB/dec for the stability of I-type system. It means:

$$K_I \le \frac{1}{T_{\Sigma i}} \tag{26}$$

where $\Delta\theta_\delta$ has an upper limit ($\Delta\theta_{\delta\_max}$) for the stability of drive system. According to (26), the larger the K_I is, the larger the cutoff frequency ω_c is, and the faster the system response is, but the smaller the phase margin is. Thus, $\Delta\theta_\delta$ has an upper limit of $\Delta\theta_{\delta\_max}$ to keep system stability.

On the other hand, the lower limit of injected d-axis current/position offset should be large enough to result in a large value of voltage terms ($\omega_r L_d \Delta i_d$, $R\Delta i_d$, and $\omega_r \psi_m \sin(\Delta\theta_\delta)$) which are related to the identified parameters, leading to a higher SNR. As discussed in [11] and [20], the SNR of machine drive system can be expressed by (27):

$$\mathrm{SNR_{dB}} = 20\log_{10}\left(\frac{V_{dc}/\sqrt{3}}{V_N}\right) \tag{27}$$

where V_{dc} and V_N are the DC supply voltage and the voltage noise, respectively. The voltage fluctuation ($\omega_r L_d \Delta i_d$, $R\Delta i_d$, and $\omega_r \psi_m \sin(\Delta\theta_\delta)$) should not be less than the voltage noise V_N in (27). Thus,

$$2\sin(\Delta\theta_\delta) \ge \frac{V_{dc}}{\sqrt{3}\times 10^{\frac{\mathrm{SNR_{dB}}}{20}}\omega_r \psi_m} \tag{28a}$$

$$\Delta i_d \ge \frac{V_{dc}}{\sqrt{3}\times 10^{\frac{\mathrm{SNR_{dB}}}{20}}\omega_r L_d}, \Delta i_d \ge \frac{V_{dc}}{\sqrt{3}\times 10^{\frac{\mathrm{SNR_{dB}}}{20}} R} \tag{28b}$$

The parameter identification errors at different amplitudes of injected d-axis currents and position offset are depicted in Figs. 7 and 8, respectively. The estimation errors become smaller with increasing amplitude of injection. For instance, when $\Delta i_d \ge 0.4$ A and $\Delta\theta_\delta \ge 3°$, the errors are small enough within acceptable accuracy. In this paper, the amplitude of d-axis current is selected as 0.5 A, and that of the position offset is selected as 5°.

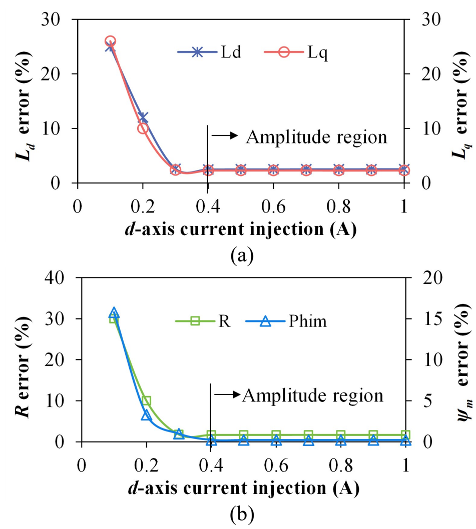

Fig. 7. Parameter identification errors at different amplitudes of injected d-axis current. (a) dq-axis inductances. (b) Stator resistance and PM flux linkage.

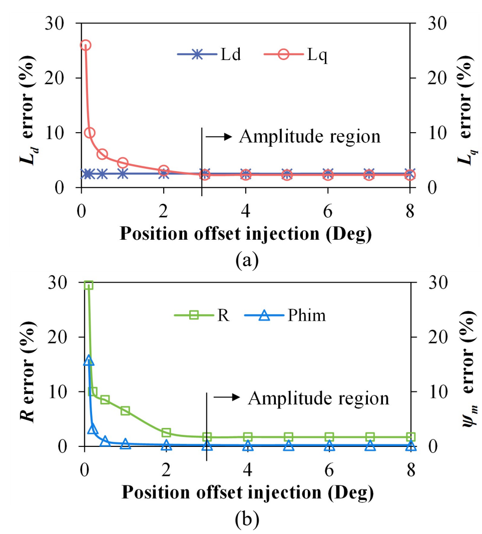

Fig. 8. Parameter identification errors at different amplitudes of injected position offset. (a) dq-axis inductances. (b) Stator resistance and PM flux linkage.

V. Experiment Results

A. Platform and Control System

To validate the proposed multi-parameter identification method under position sensorless control, experiments are carried out on an IPMSM drive platform. The control algorithm is implemented based on a dSPACE DS1006 platform, which is shown in Fig. 9. The switching frequency is set as 10 kHz. The parameters of the tested IPMSM are shown in Table III. The method in [37] is adopted for adaptive compensation of inverter nonlinearity. The three-phase currents and fast Fourier transform (FFT) analysis of A-phase current without/with inverter nonlinearity compensation are shown in Fig. 10, respectively. After compensating for inverter nonlinearity, the 5th and 7th harmonics of A-phase current are significantly reduced.

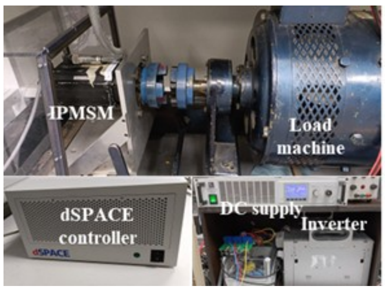

Fig. 9. Experimental test rig.

TABLE III
IPMSM Parameters

Parameters	Values
Rated speed, N_r /(r·min^{-1})	1000
Rated power, P/W	400
Rated current, I/A	4
Resistance, R/Ω	6
PM flux linkage, ψ_m /Wb	0.2505
d-axis inductance, L_d /mH	40.0
q-axis inductance, L_q /mH	60.0

B. Multi-parameter Identification Results

The multi-parameter identification results of the proposed method are presented in this section. Fig. 11 shows that 1 Hz d-axis current and rotor position offset are injected. In this paper, the signal injection is for changing the machine state. Therefore, the injection duration of signal cannot be too short, otherwise, the injection is unable to generate effective disturbance required for parameter identification.

Fig. 12 shows the waveforms of currents, voltages, identified stator inductances, stator resistance, PM flux linkage, and position estimation error. Figs. 12(a) and 12(b) show that d-axis current and dq-axis voltage fluctuate with d-axis current injection, but the effect on q-axis current can be negligible after parameters are identified. Thus, the dual signal injection basically does not cause torque ripple. As shown in Fig. 12(c), the identified dq-axis inductances, stator resistance, and PM flux linkage converge to 42.76 mH, 55.13 mH, 6.10 Ω, and 0.2501 Wb quickly, and the identification errors

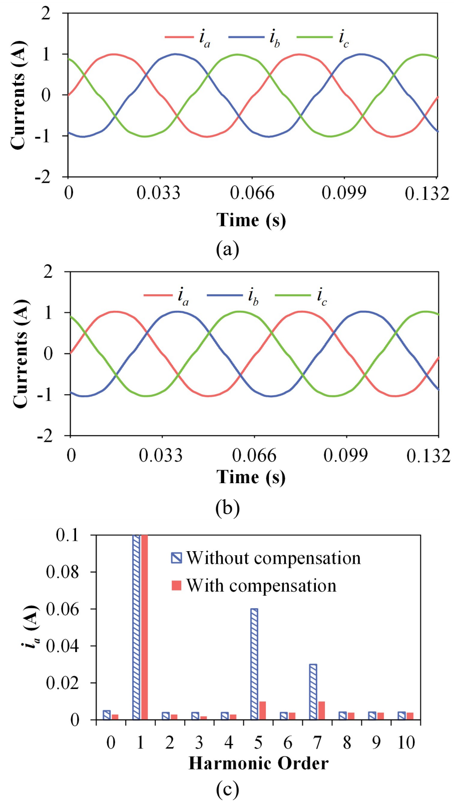

Fig. 10. VSI nonlinearity compensation. (a) Currents without compensation (4 μs dead time). (b) Currents with compensation. (c) FFT analysis of A-phase current without/ with compensation.

are 1.8%, 2.1%, 1.7%, and 0.16%, respectively. In Fig. 12(d), the identified q-axis inductance and stator resistance are fed back to position observer, and then, the position error is quickly reduced.

It is worth noting that the sampled data are processed through a low-pass filter, which effectively eliminates high-order harmonics. Consequently, the harmonics introduced by different switching frequencies have no influence on the accuracy of the parameter identification results.

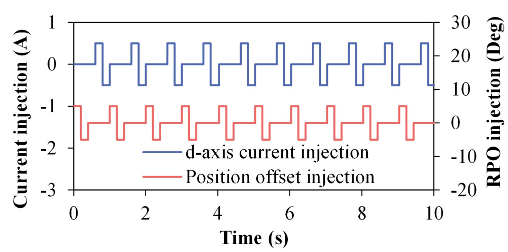

Fig. 11. Injection of d-axis current and rotor position offset.

Fig. 13 shows the waveform of identified stator inductances. In Fig. 13(b), the identified d-axis inductance increases with the increase of demagnetization current and tends to be constant when $i_d \leq -1$ A. This is because when $i_d = 0$, the iron core is saturated, and with the increase of demagnetization current, the iron core exits the saturation state. The identified q-axis inductance decreases with the increase of q-axis current due to magnetic saturation. The identified errors of dq-axis inductances remain low, and the maximum error is about 5%.

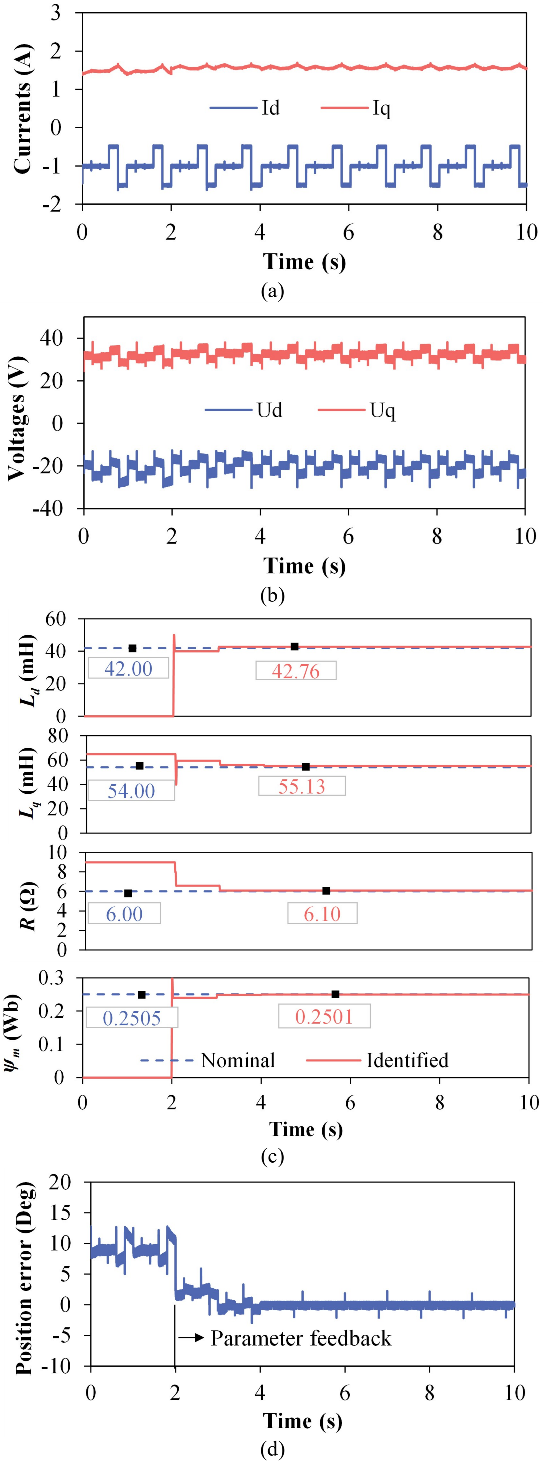

Fig. 12. Identified parameters at 400 r/min. (a) Currents. (b) Voltages. (c) Identified parameters. (d) Position estimation error.

In Fig. 14(b), identification error of stator resistance decreases with increasing dq-axis currents. This can be explained by the fact that with the increase of dq-axis currents, the proportion of the resistance voltage term to supply voltage will increase, leading to more accurate identification results. Fig. 15 shows PM flux linkage identification results at different currents. As can be seen, the identification error always keeps in a low level at different dq-axis currents.

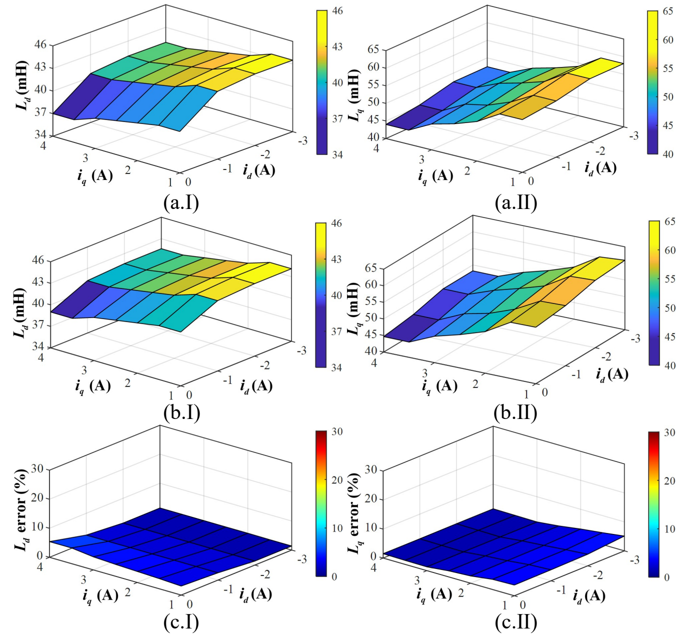

Fig. 13. Stator inductance identification maps of (I) L_d and (II) L_q. (a) FEA. (b) Identification maps. (c) Errors between FEA and identification.

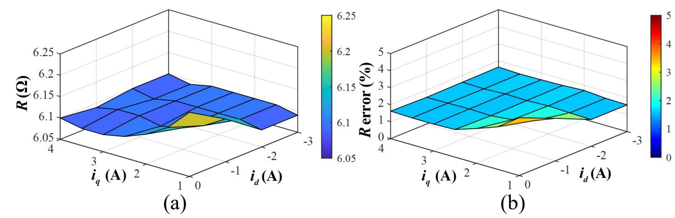

Fig. 14. Stator resistance identification. (a) Identification map. (b) Error map.

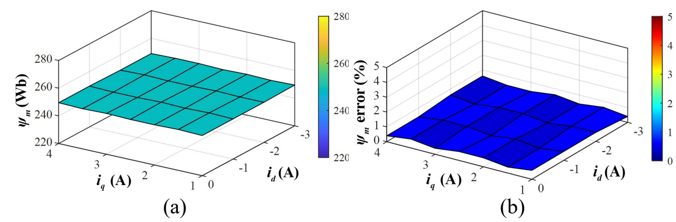

Fig. 15. PM flux linkage identification. (a) Identification map. (b) Error map.

C. Comparison Results

In order to further present that the proposed parameter identification method has the superiority in suppressing position error and solving the rank-deficiency problem, it is compared with two conventional methods in [21] and [32], named as conventional 1 and conventional 2, respectively.

Firstly, as discussed in part A of Section III, the full-rank estimation model in [21] is employed to identify stator resistance, inductance, and PM flux linkage, which does not consider the influence of position error on parameter identification. Fig. 16 shows that with the increase of initial position error, the parameter identification errors of conventional method 1 also increase. However, the identification error of the proposed method remains unchanged, which demonstrates the effectiveness of the proposed method in suppressing position errors.

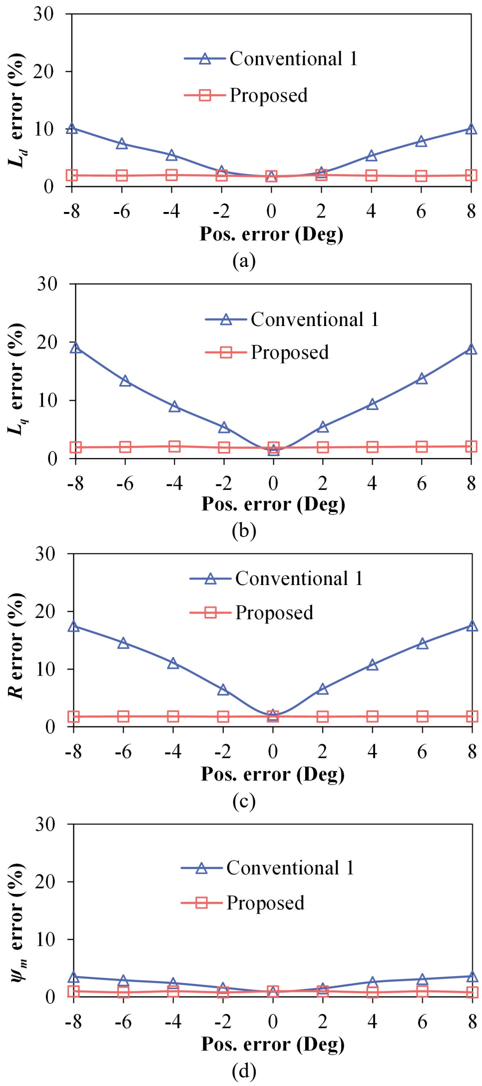

Fig. 16. Parameter identification errors at different initial position errors. (a) d-axis inductance. (b) q-axis inductance. (c) Stator resistance. (d) PM flux linkage.

Secondly, with the help of solving a multivariate nonlinear regression problem, the parameter identification model without the influence of position error is established in [32], i.e., conventional method 2. Then, a three-step pulse current is injected into d-axis to construct the identification model, which is rank-deficient. It is easy to cause the solutions of identified parameters to be trapped in local optima, as discussed in part B of Section III.

Fig. 17 shows the comparison of parameter identification results between conventional 2 and proposed methods. For conventional 2 method, L_q and ψ_m are estimated with a huge identification error because of rank-deficiency issue, which is consistent with the discussion in part B of Section III. There is no rank-deficiency issue for R identification, but position estimation error will deteriorate R identification. For the proposed method, all the identified parameters can rapidly converge to the nominal value. Thus, by dual signal alternate injection, the proposed method can identify L_d, L_q, R, and ψ_m simultaneously with high accuracy.

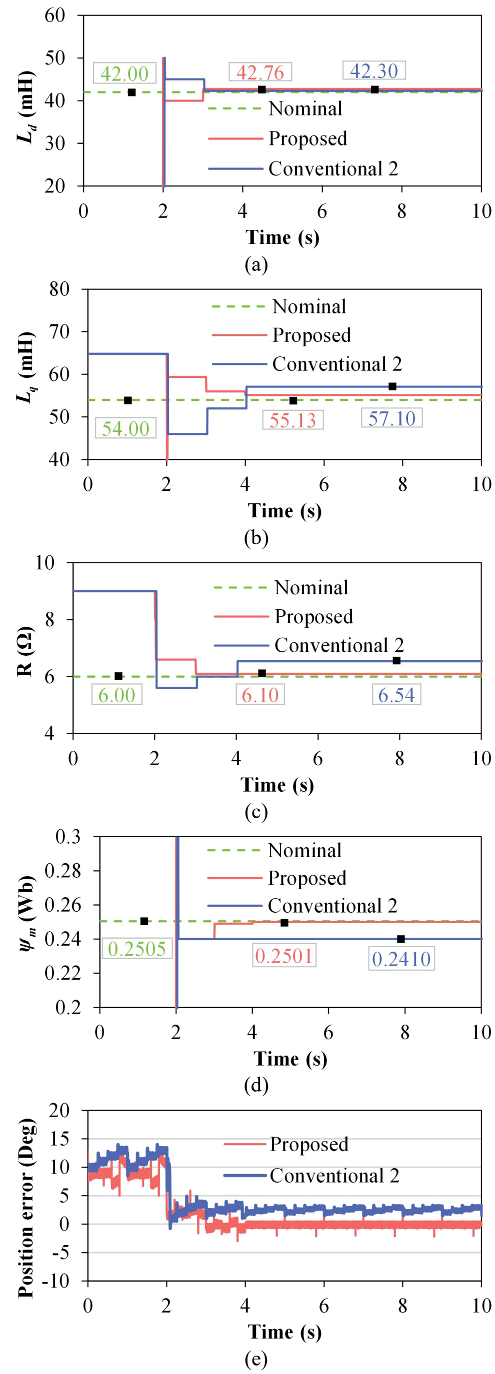

Fig. 17. Comparison of parameter identification between conventional 2 and proposed methods. (a) L_d. (b) L_q. (c) R. (d) ψ_m. (e) Position observation error.

VI. Conclusion

This paper has proposed an online simultaneous multi-parameter identification method of IPMSMs under fundamental model-based sensorless control. The proposed identification model combining dq-axis voltage equations can eliminate the position error term, resulting in suppressing the influence of position error on parameter identification. To address rank-deficiency issue, this paper has proposed a novel dual signal alternate injection method, i.e., a zero, positive, and negative d-axis current injection together with a position offset injection, respectively. Utilizing a gradient descent-based least square algorithm, the parameters, including stator resistance, dq-axis inductances, and PM flux linkage, have been identified simultaneously by sampling currents and voltages. The proposed method can be generally applied to IPMSMs under different dq-axis current conditions, which is validated experimentally.

It is worth noting that the proposed parameter identification method can be applicable to both SPMSMs and IPMSMs.

References

[1] P. Wang, Z. Q. Zhu, and D. W. Liang, "Virtual Back-EMF Injection Based Online Parameter Identification of Surface-mounted PMSMs under Sensorless Control," *IEEE Trans. on Ind. Electron.*, vol. 72, no. 6, pp. 5579–5590, Jun. 2025.

[2] P. Wang, Z. Q. Zhu, and D. W. Liang, "A Novel Virtual Flux Linkage Injection Method for Online Monitoring PM Flux Linkage and Temperature of DTP-SPMSMs under Sensorless Control," *IEEE Trans. on Ind. Electron.*, pp. 1–15, Jul. 2025.

[3] G. D. Bi, Q. W. Wang, and D. W. Ding *et al.*, "Multi-optimization Objective Online Tracking-based Parameter Self-tuning Method for Sensorless PMSM Drives," *IEEE Trans. on Transp. Electrific.*, vol. 9, no. 1, pp. 1390–1402, Mar. 2023.

[4] Z. Y. Liu, Y. Han, and G. D. Feng *et al.*, "Efficient Nonlinear Multi-parameter Decoupled Estimation of PMSM Drives based on Multi-state Voltage and Torque Measurements," *IEEE Trans. on Energy Convers.*, vol. 38, no. 1, pp. 321–331, Mar. 2023.

[5] K. Choi, Y. H. Kim, and K. S. Kim *et al.*, "Using the Stator Current Ripple Model for Real-time Estimation of Full Parameters of a Permanent Magnet Synchronous Motor," *IEEE Access*, vol. 7, pp. 33369–33379, Mar. 2019.

[6] K. Liu, Q. Zhang, and J. T. Chen *et al.*, "Online Multiparameter Estimation of Nonsalient-pole PM Synchronous Machines with Temperature Variation Tracking," *IEEE Trans. on Ind. Electron.*, vol. 58, no. 5, pp. 1776–1788, May 2011.

[7] S. J. Underwood, and I. Husain, "Online Parameter Estimation and Adaptive Control of PMSMs," *IEEE Trans. on Ind. Electron.*, vol. 57, no. 7, pp. 2435–2443, Jul. 2010.

[8] G. D. Feng, C. Y. Lai, and K. Mukherjee *et al.*, "Current Injection-based Online Parameter and VSI Nonlinearity Estimation for PMSM Drives Using Current and Voltage DC Components," *IEEE Trans. on Transp. Electrific.*, vol. 2, no. 2, pp. 119–128, Jun. 2016.

[9] K. Liu, and Z. Q. Zhu, "Position-offset-based Parameter Estimation Using the Adaline NN for Condition Monitoring of PMSMs," *IEEE Trans. on Ind. Electron.*, vol. 62, no. 4, pp. 2372–2383, Apr. 2015.

[10] K. Liu, and Z. Q. Zhu, "Position Offset-based Parameter Estimation for Permanent Magnet Synchronous Machines under Variable Speed Control," *IEEE Trans. on Power Electron.*, vol. 30, no. 6, pp. 3438–3446, Jun. 2015.

[11] P. Wang, Z. Q. Zhu, and D. W. Liang, "Improved Position-offset based Online Parameter Estimation of PMSMs under Constant and Variable Speed Operations," *IEEE Trans. on Energy Convers.*, vol. 39, no. 2, pp. 1325–1340, Jun. 2024.

[12] C. Y. Lai, G. D. Feng, and Z. Li *et al.*, "Computation-efficient Decoupled Multiparameter Estimation of PMSMs from Massive Redundant Measurements," *IEEE Trans. on Power Electron.*, vol. 35, no. 10, pp. 10729–10740, Oct. 2020.

[13] P. L. Jansen, and R. D. Lorenz, "Transducerless Position and Velocity Estimation in Induction and Salient AC Machines," *IEEE Trans. on Ind. Appl.*, vol. 31, no. 2, pp. 240–247, Mar.-Apr. 1995.

[14] J. H. Jang, S. K. Sul, and J. I. Ha *et al.*, "Sensorless Drive of Surface-mounted Permanent-magnet Motor by High-frequency Signal Injection based on Magnetic Saliency," *IEEE Trans. on Ind. Appl.*, vol. 39, no. 4, pp. 1031–1039, Jul.-Aug. 2003.

[15] Z. Q. Chen, M. Tomita, and S. Doki *et al.*, "An Extended Electromotive Force Model for Sensorless Control of Interior Permanent-magnet Synchronous Motors," *IEEE Trans. on Ind. Electron.*, vol. 50, no. 2, pp. 288–295, Apr. 2003.

[16] S. G. Mei, W. Z. Lu, and Q. G. Fan *et al.*, "Sensorless Control Strategy of Permanent Magnet Synchronous Motor based on Error Compensation Estimated by Sliding Mode Observer," *Trans. of China Electrotech. Soc.*, vol. 38, no. 2, pp. 398–408, Jan. 2023.

[17] C. C. Wang, L. F. Gou, and M. L. Zhou *et al.*, "Sensorless Control of IPMSM based on Improved Discrete Second-order Sliding Mode Observer," *Trans. of China Electrotech. Soc.*, vol. 38, no. 2, pp. 387–397, Jan. 2023.

[18] X. Fang, L. M. Wang, and K. Zhang, "High Order Nonsingular Fast Terminal Sliding Mode Control of Permanent Magnet Linear Motor based on Disturbance Observer," *Trans. of China Electrotech. Soc.*, vol. 38, no. 2, pp. 409–421, Jan. 2023.

[19] P. Wang, Z. Q. Zhu, and Z. B. Feng, "Virtual Back EMF Injection-based Online Full-parameter Estimation of DTP-SPMSMs under Sensorless Control," *IEEE Trans. on Transp. Electrific.*, vol. 11, no. 4, pp. 9823–9837, Aug. 2025.

[20] Z. Q. Zhu, P. Wang, and N. M. A. Freire *et al.*, "A Novel Rotor Position-offset Injection-based Online Parameter Estimation of Sensorless Controlled Surface-mounted PMSMs", *IEEE Trans. on Energy Convers.*, vol. 39, no. 3, pp. 1930–1946, Sept. 2024.

[21] M. S. Rafaq, F. Mwasilu, and J. Kim *et al.*, "Online Parameter Identification for Model-based Sensorless Control of Interior Permanent Magnet Synchronous Machine," *IEEE Trans. on Power Electron.*, vol. 32, no. 6, pp. 4631–4643, Jun. 2017.

[22] Y. F. Hu, K. Liu, and W. Hua *et al.*, "First-order Model Based Inductance Identification with Least Square Method for High-speed Sensorless Control of Permanent Magnet Synchronous Machines," *IEEE Trans. on Power Electron.*, vol. 38, no. 7, pp. 8719–8729, Jul. 2023.

[23] O. C. Kivanc, and S. B. Ozturk, "Sensorless PMSM Drive based on Stator Feedforward Voltage Estimation Improved with MRAS Multiparameter Estimation," *IEEE/ASME Trans. on Mechatron.*, vol. 23, no. 3, pp. 1326–1337, Jun. 2018.

[24] Y. Yao, Y. K. Huang, and F. Peng *et al.*, "Position Sensorless Drive and Online Parameter Estimation for Surface-mounted PMSMs based on Adaptive Full-state Feedback Control," *IEEE Trans. on Power Electron.*, vol. 35, no. 7, pp. 7341–7355, Jul. 2020.

[25] M. A. Hamida, J. De Leon, and A. Glumineau *et al.*, "An Adaptive Interconnected Observer for Sensorless Control of PM Synchronous Motors with Online Parameter Identification," *IEEE Trans. on Ind. Electron.*, vol. 60, no. 2, pp. 739–748, Feb. 2013.

[26] S. B. Liu, Q. W. Wang, and G. Q. Zhang *et al.*, "Online Temperature Identification Strategy for Position Sensorless PMSM Drives with Position Error Adaptive Compensation," *IEEE Trans. Power Electron.*, vol. 37, no. 7, pp. 8502–8512, Jul. 2022.

[27] T. Y. Liu, Z. Q. Zhu, and B. Shuang *et al.*, "An Online Position Error Correction Method for Sensorless Control of PMSM with Parameter Mismatch," *IEEE Access*, vol. 9, pp. 135708–135722, Sept. 2021.

[28] S. Ichikawa, M. Tomita, and S. Doki *et al.*, "Sensorless Control of Permanent-magnet Synchronous Motors Using Online Parameter Identification based on System Identification Theory," *IEEE Trans. on Ind. Electron.*, vol. 53, no. 2, pp. 363–372, Apr. 2006.

[29] S. Ichikawa, M. Tomita, and S. Doki *et al.*, "Sensorless Control of Synchronous Reluctance Motors based on Extended EMF Models Considering Magnetic Saturation with Online Parameter Identification," *IEEE Trans. on Ind. Appl.*, vol. 42, no. 5, pp. 1264–1274, Sept. 2006.

[30] G. D. Feng, C. Y. Lai, and J. Tjong *et al.*, "Exploring the Phase Angle of Measured Speed Harmonic for Efficient Permanent Magnet Temperature Estimation of PMSMs," *IEEE Trans. on Energy Convers.*, vol. 34, no. 3, pp. 1475–1484, Sept. 2019.

[31] W. T. Deng, C. L. Xia, and Y. Yan *et al.*, "Online Multiparameter Identification of Surface-mounted PMSM Considering Inverter Disturbance Voltage," *IEEE Trans. on Energy Convers.*, vol. 32, no. 1, pp. 202–212, Mar. 2017.

[32] Y. R. Wang, Y. X. Xu, and J. B. Zou, "Online Multiparameter Identification Method for Sensorless Control of SPMSM," *IEEE Trans. on Power Electron.*, vol. 35, no. 10, pp. 10601–10613, Oct. 2020.

[33] S. Morimoto, M. Sanada, and Y. Takeda, "Mechanical Sensorless Drives of IPMSM with Online Parameter Identification," *IEEE Trans. on Ind. Appl.*, vol. 42, no. 5, pp. 1241–1248, Sept.-Oct. 2006.

[34] C. Wu, Y. W. Zhao, and M. X. Sun, "Enhancing Low-speed Sensorless Control of PMSM Using Phase Voltage Measurements and Online Multiple Parameter Identification," *IEEE Trans. on Power Electron.*, vol. 35, no. 10, pp. 10700–10710, Oct. 2020.

[35] S. Morimoto, K. Kawamoto, and M. Sanada *et al.*, "Sensorless Control Strategy for Salient-pole PMSM based on Extended EMF in Rotating Reference Frame," *IEEE Trans. on Ind. Appl.*, vol. 38, no. 4, pp. 1054–1061, Jul.-Aug. 2002.

[36] P. Wang, Z. Q. Zhu, and Z. B. Feng, "Novel Virtual Active Flux Injection-based Position Error Adaptive Correction of DTP-IPMSMs under Sensorless Control," *IEEE Trans. on Transp. Electrific.*, vol. 11, no. 5, pp. 11728–11742, Oct. 2025.

[37] Y. Park, and S. K. Sul, "A Novel Method Utilizing Trapezoidal Voltage to Compensate for Inverter Nonlinearity," *IEEE Trans. on Power Electron.*, vol. 27, no. 12, pp. 4837–4846, Dec. 2012.

Peng Wang (Member, IEEE) received the M.Sc. degree in electrical engineering from Southeast University, Nanjing, China, in 2021, and the Ph.D. degree in electrical engineering from the University of Sheffield, Sheffield, UK, in 2025, respectively. Since 2025, he has been a research associate at the University of Manchester, Manchester, UK.

His current research interests include constrained optimal control, online parameter estimation, and a multi-three-phase drive system of permanent magnet synchronous machines.

Z. Q. Zhu (M'90, SM'00, F'09) received the B.Eng. and M.Sc. degrees from Zhejiang University, Hangzhou, China, in 1982 and 1984, respectively, and the Ph.D. degree from the University of Sheffield, Sheffield, UK, in 1991, all in electrical engineering. From 1988 to 2025, he was with the University of Sheffield, as Professor (1997-2025), Royal Academy of Engineering/Siemens Research Chair (2014-2023), and Head of the Electrical Machines and Drives Research Group (2008-2025). Since 2025, he has been Chair Professor at the Hong Kong Polytechnic University. He is Funding Directors of four industrial research centers, including Sheffield Siemens Gamesa Renewable Energy Research Centre and Midea Shanghai Electric Machines and Control Systems Research Centre. His current major research interests include design and control of permanent magnet machines and drives for applications ranging from electrified transportation through renewable energy to domestic appliance, robots, and automation. He is a Fellow of Royal Academy of Engineering, U.K., Institute of Electrical and Electronics Engineers (IEEE), U.S.A., Institute of Engineering and Technology (IET), U.K., and Chinese Society for Electrical Engineering (CSEE) and China Electrotechnical Society (CES).

Nuno M. A. Freire was born in Coimbra, Portugal, in 1987. He received the M.Sc. and Ph.D. degrees in electrical engineering from the University of Coimbra, Portugal, in 2010 and 2014. From 2013 to 2017, he was with Siemens Wind Power in Denmark. Since 2017, he has been with Siemens Gamesa Renewable Energy, being team leader of generator control technology development. His research interests include control and condition monitoring of electric drives applied to wind energy conversion systems.

Ziad Azar received the B.Eng. degree in electrical engineering from the University of Damascus, Damascus, Syria, in 2003, and the M.Sc. degree in electronic and electrical engineering and the Ph.D. degree in electrical engineering from the University of Sheffield, Sheffield, UK, in 2008 and 2012, respectively. In 2012, he joined Siemens Games Renewable Energy Ltd., where he is currently the Generator Team Manager with the Technology Development Department, with a focus on maturing and developing new technologies for direct-drive wind power generators. His major research interests include the modeling, design, and analysis of permanent-magnet and magnetless brushless machines for wind power applications.

Ximeng Wu received the B.Eng. degree in electrical engineering from Hefei University of Technology, Hefei, China, in 2011, and M.Sc. and Ph.D. degrees from The University of Sheffield, Sheffield, UK in 2016 and 2020, respectively. He is currently with Siemens Gamesa Renewable Energy at the University of Sheffield. His research interests include the control of permanent magnet synchronous machines.

Dawei Liang (M'22) received the B.Eng. degree from Harbin Institute of Technology, Harbin, China, in 2014, the M.Sc. degree from Karlsruhe Institute of Technology, Karlsruhe, Germany, in 2018, and the Ph.D. degree from The University of Sheffield, Sheffield, UK, in 2022, all in electrical engineering.

Since 2022, he has been a research associate with The University of Sheffield, Sheffield, UK. His research interests include thermal modelling and management, and parameter identification of electrical machines.